with displacement vector 1/4[110], identical to the defects previously identified in the ringwoodite of the meteorite Tenham[9–11]. Closer to the centre, the grains become larger (several micrometres), planar defects are no longer visible but numerous straight dislocations aligned along ⟨110⟩ directions are present.

In conclusion, transmission electron microscopy has shown that processes taking place in fayalite inside a laser-heated diamond-anvil cell are rather complex and range from melting and olivine glass formation during rapid quench to solid state transition to spinel. Note that the observed phases: glass with small idiomorphic crystals and mosaic spinel polycrystal with antiphase boundaries are very similar to those found in shocked hypersthene chondrites.

We thank Dr H. Takei for the fayalite and C. Guillemin for help with the electron microscopy. This work was supported by INAG (ATP Geodynamique 1979). Contribution IPG NS 417.

Received 14 July; accepted 23 September 1980.

1. Bassett, W. A. *A. Rev. Earth planet. Sci.* **7**, 357–384 (1979).
2. Bell, P. M. *Rev. Geophys. Space Phys.* **17**, 788–791 (1979).
3. Takei, H. *J. Cryst. Growth* **43**, 463–468 (1978).
4. Ohtani, E. *J. Phys. Earth* **27**, 189–208 (1979).
5. Jeanloz, R. *et al. Science* **197**, 457–459 (1979).
6. Gilman, J. J. *Phys. Today* 46–53 (1979).
7. Jaeger, J. C. & Starfield, A. M. *An Introduction to Applied Mathematics*, 435 (Oxford University Press, 1974).
8. Poirier, J. P. *Anelastic Properties and Related Processes in the Earth's Mantle* (AGU Monograph, in the press).
9. Poirier, J. P. & Madon, M. *EOS* **60**, 370 (1979).
10. Madon, M. & Poirier, J. P. *Science* **207**, 66–68 (1980).
11. Putnis, A. & Price, G. D. *Nature* **280**, 217–218 (1979).

Phytoplankton patchiness indicates the fluctuation spectrum of mesoscale oceanic structure

J. F. R. Gower*, K. L. Denman* & R. J. Holyer†

* Institute of Ocean Sciences, PO Box 6000, Sidney, British Columbia, Canada V8L 4B2

† Oceanography Division, Naval Ocean Research and Development Activity, NSTL Station, Mississippi 39529

Satellite imagery and large-scale oceanic experiments have replaced traditional concepts of broad sluggish currents moving throughout the ocean by the concept of a continuous distribution of more energetic eddies, the dominant eddies having space scales[1,2] of the order of 100 km. Near the ocean boundaries in such areas as the Gulf Stream and the California Current, these eddies exhibit strong thermal contrast, of the order of 2–6 °C, and their structure and distribution can be mapped using satellite thermal IR imagery[3,4]. Over most of the ocean, however, the thermal contrasts are much lower, of the order of 0.1–0.5 °C, and tend to be masked from satellite observation by small-scale atmospheric variations. To map the structure associated with mesoscale horizontal water motions in these areas, another indicator must be used for observation from space. We present here the first results of spectral analysis of satellite imagery of what we believe is phytoplankton patchiness controlled by mesoscale (10–100 km) water motions.

The surface layer of the ocean is inhabited by organisms ranging in scale from plankton (~1 μm) to whales (~10 m). Whereas whales often migrate over hemispheric distances, phytoplankton, the microscopic plants in the ocean, have the least mobility, limited to vertical migration over a few metres per day[5] accomplished by buoyancy changes. The phytoplankton may, therefore, be considered as a passive scalar being advected about by the variable ocean currents. Phytoplankton do, however, grow and reproduce; a healthy population can double its biomass in a time period of the order of 1 day[6]. Several models have been developed to describe growing phytoplankton patches being redistributed and diffused horizontally by a partially turbulent ocean[7–9]. These models have tried to describe the observed spatial variations of biomass in terms of wavenumber spectra. It has recently been concluded[7,8,10] that shipborne sampling cannot achieve sufficient spatial coverage in times short enough to be considered synoptic and that airborne or satellite sampling is required.

The biomass of phytoplankton is usually quantified by determining the amount of chlorophyll *a* pigment present. Remote measurement of chlorophyll concentration uses the colour changes caused by the combination of absorption or fluorescence of chlorophyll pigments and backscattering by associated suspended matter[11–15]. Variations in phytoplankton concentration cause measurable changes in the intensity and spectral distribution of visible light backscattered from the ocean, especially in the blue and green bands where water transmission is a maximum. Normal, low plankton concentrations cause colour changes which can be detected from space only by using specialized processing on selected wavelength bands to remove atmospheric effects. The Coastal Zone Colour Scanner on Nimbus 7 is now available as a sensor designed for this purpose. Areas of high chlorophyll concentration, however, can give large changes in water reflectivity detectable by less sophisticated systems.

Figure 1 shows an area of the ocean 180×250 km in size, south of Iceland, as imaged by the LANDSAT multispectral scanner on 19 June 1976. The image shown is a mosaic of spectral band 4 from frames 2514–12015 and 2514–12021. Band 4 is the shortest wavelength band on the instrument, covering 500–600 nm, corresponding roughly to green light. The south-west coast of Iceland is visible at the top of the image, and the 400-m depth contour crosses the middle of the scene. The land is partly cloud covered and some bands of cloud are visible at the lower right. The island of Westmannaeyjar can be seen just off the coast with the volcanic island, Surtsey, to its south-west. The swirls and eddies in the remaining area of the water show a structure characteristic of mesoscale turbulence as observed in satellite thermal imagery. This structure is much less visible in the red band, while the longest wavelength band 7 (800–1,100 nm) shows only the clouds above featureless dark water. Because this band-spectral signature is typical of suspended matter in the ocean, we interpret the eddy patterns in Fig. 1 as representing the distribution of phytoplankton biomass or of detritus derived from phytoplankton.

A phytoplankton survey tow was made in the area as part of a programme of the Institute for Marine Environmental Research, UK, on the day this image was taken. The ship travelled westwards parallel to the coast ~20-km offshore passing between Westmannaeyjar and Surtsey. The concentration of phytoplankton observed was well below average for the time of year confirming, at least, that the darker area near the top of the image corresponds to a low concentration of phytoplankton. Measurements made along the same line six weeks earlier, however, showed the strongest phytoplankton bloom observed in this area during May for five years. Repeated measurements made on a section to the west of Westmannaeyjar by staff of the Marine Research Institute of Reykjavik[16] showed that the main peak of growth in this area also occurred about a month earlier. Their data for 1976–78 show that the blooms tend to occur earlier in the shallower water on the continental shelf than in the deeper water offshore where the bloom in Fig. 1 is observed. These data also showed that an exceptionally high productivity of phytoplankton occurred in the spring of 1976. The available data, then, confirm strong productivity near this place and time and do not invalidate our interpretation of Fig. 1 as showing the effects of a phytoplankton bloom. The area of the bloom covers at least 180×180 km, the area of a single frame of LANDSAT imagery. The increase in reflectance cause by the bloom is high, but not unreasonable for plankton of the appropriate species[11] or in the appropriate stage of development[17]. No other LANDSAT scenes were collected over the area near this time

0028–0836/80/460157—03$01.00

except for an image overlapping the area of Fig. 1 but farther east, largely cloud covered, recorded on 30 May. This image shows no discernible bloom. Scarcity of satellite data is largely due to there having been no satellite receiving station capable of receiving directly image data of Iceland.

The characteristic spatial scales of the eddies and ocean turbulence structure can best be determined from a two-dimensional spectral analysis[18] of the image in which we assume that the increase in pixel value over the level for clear water is proportional to phytoplankton concentration. The resulting power spectrum can then be averaged over all directions to get a spectrum as a function of a nondirectional wave number[19].

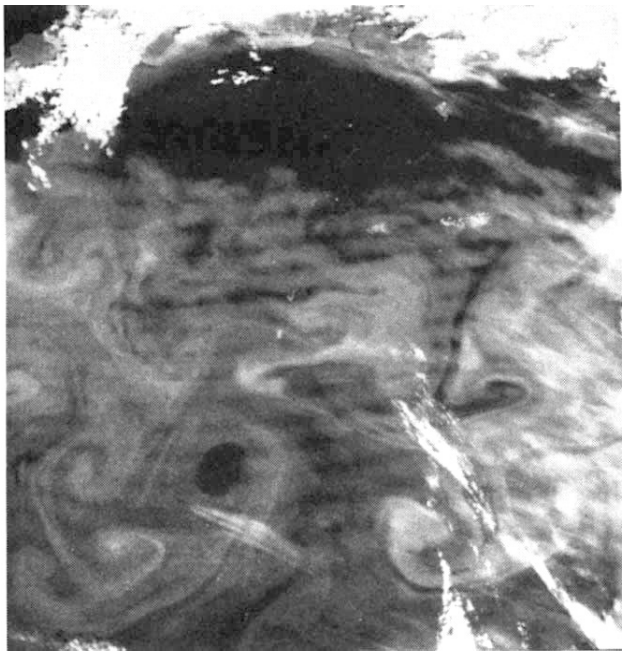

Fig. 1 Enhanced image formed from two LANDSAT Multispectral Scanner band 4 frames showing increased reflectance in the Atlantic Ocean south of Iceland on 19 June 1976. The patterns are interpreted as due to a plankton bloom in water advected by ocean mesoscale turbulence.

Before beginning this analysis, the effects of cloud were reduced by subtracting the band 7 image, suitably scaled, from the band 4 image. As water looks very dark in band 7 (near IR), the subtraction is equivalent to removing the light backscattered by aerosol particles in thin clouds and haze above the water. This scaling allows for the different instrument gain and solar irradiance between bands 4 and 7 and also, in effect, selects different values of mean Angstrom coefficient for the spectral dependence of aerosol scattering in the scene[20]. The scaling constant was adjusted to reduce the visibility of cloud features in the band 4 image. In ~10% of the area of Fig. 1 analysed, thin cloud contributed an additional 15–30% to the radiance enhancement in band 4 that is due to light scatterers in the water. The subtraction reduced this cloud contribution to ~5%. Less correction is possible in areas with thicker cloud, but these were largely avoided in the analysis.

Picture elements in the raw image are spaced on a grid with element spacing 57 × 79 m. The pixel values were averaged over groups of 8 × 6 pixels to reduce instrument noise and to give a roughly square grid of about 474-m spacing for further processing. Three overlapping areas of 256 × 256 averaged pixels each about 120 km square were then selected for Fourier transforming. The mean pixel value for each was subtracted from each pixel in the area, and the areas were Hanned (weighted with a cosine taper in both dimensions) to reduce edge effects. Although the three areas overlapped by ~55%, the Hanning reduced the correlation of the coefficients of the resulting transforms to ~25%, low enough for reasonable statistical independence. The Fourier transforms of the pixel arrays were then converted to power or signal-variance spectra, and circular ring areas in the transform plane were summed and normalized by their areas to give non-directional estimates of the variance as a function of wavelength. Wedge-shaped areas were similarly summed to give estimates of the directional effects in the water or introduced by residual cloud signals. These were found to be <10% except at the shortest wavelengths (<3 km) where a larger value (up to 20%) appears in the direction range appropriate to the cloud streaks in Fig. 1.

The logarithms of the spectral components of signal variance, averaged over all directions, are plotted in Fig. 2 against the logarithm of the inverse wavelength, K. If the spectral components are dependent on K in a power law manner, proportional to K^n, then such a plot should yield a straight line with slope n. The spectral components computed for the three areas are plotted separately and all yield a similar relation for the wavelength range 2–60 km ($K = 0.015$ to 0.5); the relations can be well fitted by straight lines. The regression line slopes are −3.11, −2.83 and −2.82 for the three areas giving an average value of −2.92. The average regression line is plotted as the dashed line in Fig. 2. At long wavelengths, the points lie below this line, but some roll off is expected for components having wavelengths comparable to the dimensions of the sample area. The point for a wavelength of 1 km lies above the line indicating reduction in slope at the short wavelength. This value may be increased by components of scene radiance due to residual cloud reflections. Variance due to small streaks of cloud such as can be seen in Fig. 1 would be expected to have more energy at the higher frequencies.

For wavelengths between 2 and 60 km the distribution of signal variance is related to inverse wavelength to the power −2.9. If the observed pixel values are interpreted as proportional to particulate backscatter from phytoplankton, then this power law also applies to the phytoplankton density and the above result can be compared with other measurements of the power law index in ocean mesoscale turbulence.

Spectra of sea-surface temperatures derived from airborne radiometer measurements have varied between −2 and −3 (refs 18, 19). Shipboard estimates of phytoplankton patchiness have varied widely, but a similar range is most typical[10,21–23]. Theoretical estimates[7–9] of the index for turbulence-controlled phytoplankton patchiness tend to be between −2 and −3. The −3 slope is consistent with the concept of two-dimensional geostrophical turbulence[24,25], where the growth rate of the phytoplankton has a negligible effect on the horizontal distribution of biomass. The signal discontinuities resulting from the small (~10) number of discrete pixel values or grey scale levels in the original image would shift the slope towards −2 (ref. 26), but this effect is reduced to a negligible amount by averaging over 48 pixels.

The relationship between phytoplankton concentration and the amount of radiance upwelling from beneath the sea surface is not in general linear. The absorption by chlorophyllous pigment increases along with the increased backscatter from the suspended planktonic matter[12,13]. In the range 500–600 nm, this leads to saturation in the reflectance values after an initial increase. Over a limited range of chlorophyll concentrations, however, the relationship can be approximated by a linear function so that the above discussion holds. The reflectance values in the areas analysed range over ~3–7% reflectance. The expected linearity of the reflectance-to-chlorophyll relation depends on the properties of the plankton actually present. The relatively high reflectivity of the water implies a high backscatter to absorption ratio, a condition which improves the linearity of the relationship.

We interpret patterns on a LANDSAT band 4 multispectral scanner image as being due to phytoplankton and show that the fluctuation spectrum is consistent with the phytoplankton dis-

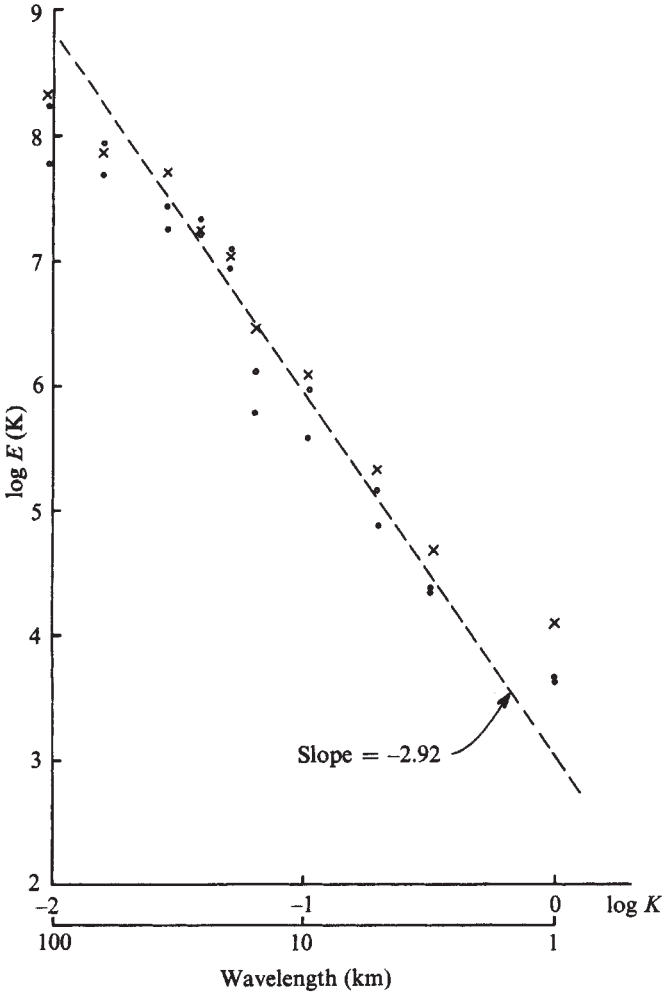

Fig. 2 Power spectra computed from three overlapping areas of Fig. 1 as described in the text. A slope of −3 in a log–log plot is characteristic of turbulent motion, and indicates that growth rate of the plankton itself is having a relatively small effect. The distribution of enhanced water reflectance in Fig. 1 should, therefore, be a useful tracer of the eddy motions.

tribution being controlled by advection in variable ocean currents, while being unaffected by their reproduction rate.

The phytoplankton are, therefore, behaving as a passive scalar and the distribution of enhanced water reflectance in Fig. 1 can be used as a tracer of eddy motion. The spatial distribution of areas showing increased reflectance can certainly be mapped more precisely from a satellite than by any other means available, and this may be why the resulting slope of the power spectrum agrees so well with theory. The problem of relating this reflectance increase to exact measures of chlorophyll concentration remains, but this should soon be possible using the improved data from NASA's Coastal Zone Colour Scanner.

In comparing satellite IR and colour mapping of ocean eddy structure both have their limitations, and the two methods will to some extent be complementary. Both methods are blocked by clouds, and both are affected by atmospheric absorption and scattering. Both measure only surface phenomena, though wind mixing, particularly at high latitudes, will tend to average properties over a surface mixed layer, often of the order of 50 m deep. Thermal measurements are more susceptible to skin effects related to the very small penetration depth ($\leq$0.1 mm) of thermal radiation. Both measurements are of ocean properties interesting and important in themselves. Taken together they can show how solar heating, water mixing and stratification, and plankton growth lead to the productivity variations that are of such importance to the world's fisheries.

Received 28 May; accepted 2 September 1980.

1. Bernstein, R. L. & White, W. B. *J. phys. Oceanogr.* **4**, 613 (1974).
2. Gould, J., Schmitz, W. J. & Wunsch, C. *Deep-Sea Res.* **21**, 911 (1974).
3. Legeckis, R. V. *J. phys. Oceanogr.* **9**, 483 (1979).
4. Bernstein, R. L., Breaker, L. & Whritner, R. *Science* **195**, 353 (1977).
5. Smayda, T. J. *Oceanogr. mar. Biol. A. Rev.* **8**, 353 (1970).
6. Eppley, R. W. *Fish Bull. U.S.* **70**, 1063 (1972).
7. Denman, K. L. & Platt, T. *J. mar. Res.* **34**, 593 (1976).
8. Denman, K. L., Okubo, A. & Platt, T. *Limnol. Oceanogr.* **22**, 1033 (1977).
9. Fasham, M. J. *Oceanogr. mar. Biol. A. Rev.* **16**, 43 (1978).
10. Horwood, J. W. *J. mar. Biol. Ass. U.K.* **58**, 487 (1978).
11. Yentsch, C. S. *Deep-Sea Res.* **7**, 1 (1960).
12. Clarke, G. L., Ewing, G. C. & Lorenzen, C. J. *Science* **167**, 1119 (1970).
13. Morel, A. & Prieur, L. *Limnol. Oceanogr.* **22**, 709 (1977).
14. Gower, J. F. R. *Boundary Layer Met.* **18**, 235 (1980).
15. Smith, R. C. & Baker, K. S. *Limnol. Oceanogr.* **23**, 247 (1978).
16. Fruigeirssin, E., Einarrson, S., Olafsson, J. & Thordandottir, T. *International Council for the Exploration of the Sea, Early Life History of Fish Symp.* (Woods Hole, 1979).
17. Kiefer, D. A., Olson, R. J. & Wilson, W. H. *Limnol. Oceanogr.* **24**, 664 (1979).
18. Saunders, P. M. *Deep-Sea Res.* **19**, 467 (1972).
19. Holladay, C. G. & O'Brien, J. J. *J. phys. Oceanogr.* **5**, 761 (1975).
20. Gordon, H. R. & Clark, D. K. *Boundary Layer Met.* **18**, 299 (1980).
21. Denman, K. L. & Platt, T. *Mem. Soc. r. Sci. Liège* **7**, 19 (1975).
22. Denman, K. L. *Deep-Sea Res.* **23**, 539 (1976).
23. Fasham, M. J. & Pugh, P. R. *Deep-Sea Res.* **23**, 527 (1976).
24. Kraichnan, R. H. *Phys. Fluids* **10**, 1417 (1976).
25. Charney, J. G. *J. atmos. Sci.* **28**, 1087 (1971).
26. Phillips, O. M. *J. phys. Oceanogr.* **1**, 1 (1971).

The nature of inherited deafness in *deafness* mice

Karen P. Steel & Gregory R. Bock

MRC Institute of Hearing Research, University of Nottingham, Nottingham NG7 2RD, UK

Many mouse mutants have an apparent deficiency in their responsiveness to sound[1]. Most of these mutants have other abnormalities in addition to their hearing deficit, and the only two which have been subjected to a detailed anatomical and physiological study, *shaker*-1 and *Ames waltzer*, also have motor abnormalities[2,3]. The existence of such motor abnormalities throws some doubt on the usefulness of these two mutants as possible models for hereditary deafness in man, which is most frequently uncomplicated[4]. Deol and Kocher have described the *deafness* mutation in which mice homozygous for the recessive *deafness* gene (*dn*/*dn*) were unresponsive to sound and had no significant behavioural abnormality[5]. Cochlear hair cells in *deafness* mice develop normally and then degenerate, and the adult animals are completely deaf[6]. We have now studied *deafness* mice in order to determine the nature of their inherited deafness. Our data indicate that stimulus-related cochlear potentials do not develop even though hair cells are present in the young animal. The endocochlear potential is present in the scala media, but behaves abnormally during anoxia.

Deafness mice were bred in our laboratory from stock obtained from M.S. Deol, University College, London. Heterozygotes (+/*dn*) were used as controls, and were distinguished from their homozygous (*dn*/*dn*) littermates by the failure of the latter to exhibit a Preyer reflex in response to a metallic click. Gross VIIIth nerve action potential thresholds for control animals are presented in Fig. 1. No action potentials could be detected in *deafness* mice in any age group at any frequency, even when 5,000 stimulus repetitions were included in the average.

Cochlear microphonics in response to discrete continuous tones between 1 kHz and 60 kHz were recorded from the same electrode and measured with a computer-controlled lock-in amplifier. No cochlear microphonic could be recorded at any age in the mutant mice, although normal microphonics with maximum amplitudes of about 100 μV were found in control animals. Resting noise levels for these measurements were below 0.1 μV.

0028–0836/80/460159—03$01.00